and so addresses a crucial problem in structural biology. This is done by the remarkably successful method of single-particle image reconstruction, in which images of the same protein, lying in random orientations within a thin film of vitreous ice, are combined in the correct orientation to form a three-dimensional reconstructed charge-density map at nanometre or better resolution. The summation over many particles achieves the same radiation-damage-reduction effect as does crystallographic redundancy in protein crystallography. Finally, Section 2.5.8 describes experience with the application of numerical direct methods to the phase problem in electron diffraction. Although direct imaging 'solves' the phase problem, there are many practical problems in combining electron-microdiffraction intensities with corresponding high-resolution images of a structure over a large tilt range. In cases where multiple scattering can be minimized, some success has therefore been obtained using direct phasing methods, as reviewed in this section.

For most inorganic materials the complications of many-beam dynamical diffraction processes prevent the direct application of these techniques of image analysis, which depend on having a linear relationship between the image intensity and the value of the projected potential distribution of the sample. The smaller sensitivities to radiation damage can, to some extent, remove the need for the application of such methods by allowing direct visualization of structure with ultra-high-resolution images and the use of microdiffraction techniques.

2.5.2. Electron diffraction and electron microscopy[1]

By J. M. Cowley

2.5.2.1. Introduction

The contributions of electron scattering to the study of the structures of crystalline solids are many and diverse. This section will deal only with the scattering of high-energy electrons (in the energy range of 10^4 to 10^6 eV) in transmission through thin samples of crystalline solids and the derivation of information on crystal structures from diffraction patterns and high-resolution images. The range of wavelengths considered is from about 0.122 Å (12.2 pm) for 10 kV electrons to 0.0087 Å (0.87 pm) for 1 MeV electrons. Given that the scattering amplitudes of atoms for electrons have much the same form and variation with $(\sin\theta)/\lambda$ as for X-rays, it is apparent that the angular range for strong scattering of electrons will be of the order of 10^{-2} rad. Only under special circumstances, usually involving multiple elastic and inelastic scattering from very thick specimens, are scattering angles of more than 10^{-1} rad of importance.

The strength of the interaction of electrons with matter is greater than that of X-rays by two or three orders of magnitude. The single-scattering, first Born approximation fails significantly for scattering from single heavy atoms. Diffracted beams from single crystals may attain intensities comparable with that of the incident beam for crystal thicknesses of 10^2 Å, rather than 10^4 Å or more. It follows that electrons may be used for the study of very thin samples, and that dynamical scattering effects, or the coherent interaction of multiply scattered electron waves, will modify the diffracted amplitudes in a significant way for all but very thin specimens containing only light atoms.

The experimental techniques for electron scattering are largely determined by the possibility of focusing electron beams by use of strong axial magnetic fields, which act as electron lenses having focal lengths as short as 1 mm or less. Electron microscopes employing such lenses have been produced with resolutions approaching 1 Å. With such instruments, images showing individual isolated atoms of moderately high atomic number may be obtained. The resolution available is sufficient to distinguish neighbouring rows of adjacent atoms in the projected structures of thin crystals viewed in favourable orientations. It is therefore possible in many cases to obtain information on the structure of crystals and of crystal defects by direct inspection of electron micrographs.

The electromagnetic electron lenses may also be used to form electron beams of very small diameter and very high intensity. In particular, by the use of cold field-emission electron guns, it is possible to obtain a current of 10^{-10} A in an electron beam of diameter 10 Å or less with a beam divergence of less than 10^{-2} rad, *i.e.* a current density of 10^4 A cm^{-2} or more. The magnitudes of the electron scattering amplitudes then imply that detectable signals may be obtained in diffraction from assemblies of fewer than 10^2 atoms. On the other hand, electron beams may readily be collimated to better than 10^{-6} rad.

The cross sections for inelastic scattering processes are, in general, less than for the elastic scattering of electrons, but signals may be obtained by the observation of electron energy losses, or the production of secondary radiations, which allow the analysis of chemical compositions or electronic excited states for regions of the crystal 100 Å or less in diameter.

On the other hand, the transfer to the sample of large amounts of energy through inelastic scattering processes produces radiation damage which may severely limit the applicability of the imaging and diffraction techniques, especially for biological and organic materials, unless the information is gathered from large specimen volumes with low incident electron beam densities.

Structure analysis of crystals can be performed using electron diffraction in the same way as with X-ray or neutron diffraction. The mathematical expressions and the procedures are much the same. However, there are peculiarities of the electron-diffraction case which should be noted.

(1) Structure analysis based on electron diffraction is possible for thin specimens for which the conditions for kinematical scattering are approached, *e.g.* for thin mosaic single-crystal specimens, for thin polycrystalline films having a preferred orientation of very small crystallites or for very extensive, very thin single crystals of biological molecules such as membranes one or a few molecules thick.

(2) Dynamical diffraction effects are used explicitly in the determination of crystal symmetry (with no Friedel's law limitations) and for the measurement of structure amplitudes with high accuracy.

(3) For many radiation-resistant materials, the structures of crystals and of some molecules may be determined directly by imaging atom positions in projections of the crystal with a resolution of 2 Å or better. The information on atom positions is not dependent on the periodicity of the crystal and so it is equally possible to determine the structures of individual crystal defects in favourable cases.

(4) Techniques of microanalysis may be applied to the determination of the chemical composition of regions of diameter 100 Å or less using the same instrument as for diffraction, so that the chemical information may be correlated directly with morphological and structural information.

(5) Crystal-structure information may be derived from regions containing as few as 10^2 or 10^3 atoms, including very small crystals and single or multiple layers of atoms on surfaces.

The material of this section is also reviewed in the text by Spence (2003).

2.5.2.2. The interactions of electrons with matter

(1) The *elastic* scattering of electrons results from the interaction of the charged electrons with the electrostatic potential distribution, $\varphi(\mathbf{r})$, of the atoms or crystals. An incident electron of kinetic energy eW gains energy $e\varphi(\mathbf{r})$ in the potential field. Alternatively it may be stated that an incident electron wave of

[1] Questions related to this section may be addressed to Professor J. C. H. Spence (see list of contributing authors).

wavelength $\lambda = h/mv$ is diffracted by a region of variable refractive index

$$n(\mathbf{r}) = k/K_0 = \{[W + \varphi(\mathbf{r})]/W\}^{1/2} \simeq 1 + \varphi(\mathbf{r})/2W.$$

(2) The most important *inelastic* scattering processes are:

(*a*) thermal diffuse scattering, with energy losses of the order of 2×10^{-2} eV, separable from the elastic scattering only with specially devised equipment; the angular distribution of thermal diffuse scattering shows variations with $(\sin\theta)/\lambda$ which are much the same as for the X-ray case in the kinematical limit;

(*b*) bulk plasmon excitation, or the excitation of collective energy states of the conduction electrons, giving energy losses of 3 to 30 eV and an angular range of scattering of 10^{-4} to 10^{-3} rad;

(*c*) surface plasmons, or the excitation of collective energy states of the conduction electrons at discontinuities of the structure, with energy losses less than those for bulk plasmons and a similar angular range of scattering;

(*d*) interband or intraband excitation of valence-shell electrons giving energy losses in the range of 1 to 10^2 eV and an angular range of scattering of 10^{-4} to 10^{-2} rad;

(*e*) inner-shell excitations, with energy losses of 10^2 eV or more and an angular range of scattering of 10^{-3} to 10^{-2} rad, depending on the energy losses involved.

(3) In the original treatment by Bethe (1928) of the elastic scattering of electrons by crystals, the Schrödinger equation is written for electrons in the periodic potential of the crystal; *i.e.*

$$\nabla^2\psi(\mathbf{r}) + K_0^2[1 + \varphi(\mathbf{r})/W]\psi(\mathbf{r}) = 0, \tag{2.5.2.1}$$

where

$$\begin{aligned}\varphi(\mathbf{r}) &= \int V(\mathbf{u}) \exp\{-2\pi i\mathbf{u}\cdot\mathbf{r}\}\,\mathrm{d}\mathbf{u} \\ &= \sum_{\mathbf{h}} V_{\mathbf{h}} \exp\{-2\pi i\mathbf{h}\cdot\mathbf{r}\},\end{aligned} \tag{2.5.2.2}$$

$\mathbf{K}_0$ is the wavevector in zero potential (outside the crystal) (magnitude $2\pi/\lambda$) and W is the accelerating voltage. The solutions of the equation are Bloch waves of the form

$$\psi(\mathbf{r}) = \sum_{\mathbf{h}} C_{\mathbf{h}}(\mathbf{k}) \exp\{-i(\mathbf{k}_0 + 2\pi\mathbf{h})\cdot\mathbf{r}\}, \tag{2.5.2.3}$$

where $\mathbf{k}_0$ is the incident wavevector in the crystal and $\mathbf{h}$ is a reciprocal-lattice vector. Substitution of (2.5.2.2) and (2.5.2.3) in (2.5.2.1) gives the dispersion equations

$$(\kappa^2 - k_{\mathbf{h}}^2)C_{\mathbf{h}} + \sum_{\mathbf{g}}{}' V_{\mathbf{h}-\mathbf{g}}C_{\mathbf{g}} = 0. \tag{2.5.2.4}$$

Here κ is the magnitude of the wavevector in a medium of constant potential V_0 (the 'inner potential' of the crystal). The refractive index of the electron in the average crystal potential is then

$$n = \kappa/K = (1 + V_0/W)^{1/2} \simeq 1 + V_0/2W. \tag{2.5.2.5}$$

Since V_0 is positive and of the order of 10 V and W is 10^4 to 10^6 V, $n - 1$ is positive and of the order of 10^{-4}.

Solution of equation (2.5.2.4) gives the Fourier coefficients $C_{\mathbf{h}}^{(i)}$ of the Bloch waves $\psi^{(i)}(\mathbf{r})$ and application of the boundary conditions gives the amplitudes of individual Bloch waves (see Chapter 5.2).

(4) The experimentally important case of transmission of high-energy electrons through thin specimens is treated on the assumption of a plane wave incident in a direction almost perpendicular to an infinitely extended plane-parallel lamellar crystal, making use of the *small-angle scattering approximation* in which the forward-scattered wave is represented in the paraboloidal approximation to the sphere. The incident-beam direction, assumed to be almost parallel to the z axis, is unique and the z component of $\mathbf{k}$ is factored out to give

$$\nabla^2\psi + 2k\sigma\varphi\psi = \pm i2k\frac{\partial\psi}{\partial z}, \tag{2.5.2.6}$$

where $k = 2\pi/\lambda$ and $\sigma = 2\pi me\lambda/h^2$. [See Lynch & Moodie (1972), Portier & Gratias (1981), Tournarie (1962), and Chapter 5.2.]

This equation is analogous to the time-dependent Schrödinger equation with z replacing t. Retention of the $\pm$ signs on the right-hand side is consistent with both ψ and ψ^* being solutions, corresponding to propagation in opposite directions with respect to the z axis. The double-valued solution is of importance in consideration of reciprocity relationships which provide the basis for the description of some dynamical diffraction symmetries. (See Section 2.5.3.)

(5) The integral form of the wave equation, commonly used for scattering problems, is written, for electron scattering, as

$$\psi(\mathbf{r}) = \psi^{(0)}(\mathbf{r}) + (\sigma/\lambda)\int \frac{\exp\{-i\mathbf{k}|\mathbf{r} - \mathbf{r}'|\}}{|\mathbf{r} - \mathbf{r}'|}\varphi(\mathbf{r}')\psi(\mathbf{r}')\,\mathrm{d}\mathbf{r}'. \tag{2.5.2.7}$$

The wavefunction $\psi(\mathbf{r})$ within the integral is approximated by using successive terms of a Born series

$$\psi(\mathbf{r}) = \psi^{(0)}(\mathbf{r}) + \psi^{(1)}(\mathbf{r}) + \psi^{(2)}(\mathbf{r}) + \ldots. \tag{2.5.2.8}$$

The first Born approximation is obtained by putting $\psi(\mathbf{r}) = \psi^{(0)}(\mathbf{r})$ in the integral and subsequent terms $\psi^{(n)}(\mathbf{r})$ are generated by putting $\psi^{(n-1)}(\mathbf{r})$ in the integral.

For an incident plane wave, $\psi^{(0)}(\mathbf{r}) = \exp\{-i\mathbf{k}_0\cdot\mathbf{r}\}$ and for a point of observation at a large distance $\mathbf{R} = \mathbf{r} - \mathbf{r}'$ from the scattering object ($|\mathbf{R}| \gg |\mathbf{r}'|$), the first Born approximation is generated as

$$\psi^{(1)}(\mathbf{r}) = \frac{i\sigma}{\lambda R}\exp\{-i\mathbf{k}\cdot\mathbf{R}\}\int \varphi(\mathbf{r}')\exp\{i\mathbf{q}\cdot\mathbf{r}'\}\,\mathrm{d}\mathbf{r}',$$

where $\mathbf{q} = \mathbf{k} - \mathbf{k}_0$ or, putting $\mathbf{u} = \mathbf{q}/2\pi$ and collecting the pre-integral terms into a parameter μ,

$$\Psi(\mathbf{u}) = \mu\int \varphi(\mathbf{r})\exp\{2\pi i\mathbf{u}\cdot\mathbf{r}\}\,\mathrm{d}\mathbf{r}. \tag{2.5.2.9}$$

This is the Fourier-transform expression which is the basis for the *kinematical scattering approximation*. It is derived on the basis that all $\psi^{(n)}(\mathbf{r})$ terms for $n \neq 0$ are very much smaller than $\psi^{(0)}(\mathbf{r})$ and so is a weak scattering approximation.

In this approximation, the scattered amplitude for an atom is related to the atomic structure amplitude, $f(\mathbf{u})$, by the relationship, derived from (2.5.2.8),

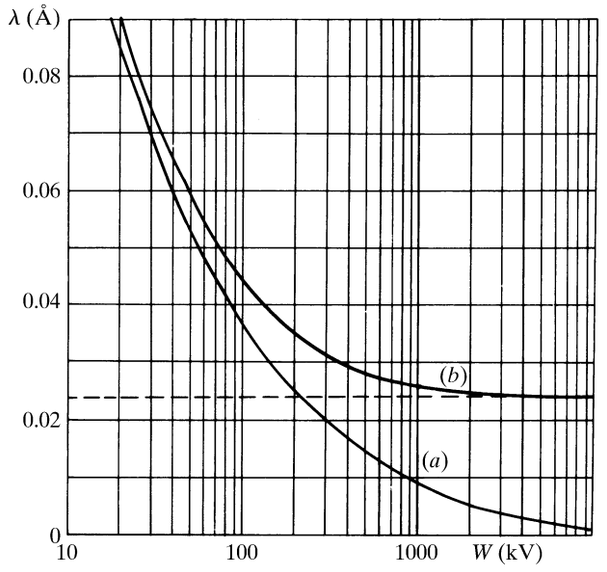

Fig. 2.5.2.1. The variation with accelerating voltage of electrons of (*a*) the wavelength, λ and (*b*) the quantity $\lambda[1 + (h^2/m_0^2c^2\lambda^2)] = \lambda_c/\beta$ which is proportional to the interaction constant σ [equation (2.5.2.14)]. The limit is the Compton wavelength λ_c (after Fujiwara, 1961).

$$\psi(\mathbf{r}) = \exp\{-i\mathbf{k}_0 \cdot \mathbf{r}\} + i\frac{\exp\{-i\mathbf{k} \cdot \mathbf{r}\}}{R\lambda}\sigma f(\mathbf{u}),$$
$$f(\mathbf{u}) = \int \varphi(\mathbf{r}) \exp\{2\pi i\mathbf{u} \cdot \mathbf{r}\}\, \mathrm{d}\mathbf{r}. \qquad (2.5.2.10)$$

For centrosymmetrical atom potential distributions, the $f(\mathbf{u})$ are real, positive and monotonically decreasing with $|\mathbf{u}|$. A measure of the extent of the validity of the first Born approximation is given by the fact that the effect of adding the higher-order terms of the Born series may be represented by replacing $f(\mathbf{u})$ in (2.5.2.10) by the complex quantities $f(\mathbf{u}) = |\mathbf{f}| \exp\{i\eta(\mathbf{u})\}$ and for single heavy atoms the phase factor η may vary from 0.2 for $|\mathbf{u}| = 0$ to 4 or 5 for large $|\mathbf{u}|$, as seen from the tables of *IT* C (2004, Section 4.3.3).

(6) Relativistic effects produce appreciable variations of the parameters used above for the range of electron energies considered. The relativistic values are

$$m = m_0(1 - v^2/c^2)^{-1/2} = m_0(1 - \beta^2)^{-1/2}, \qquad (2.5.2.11)$$
$$\lambda = h[2m_0|e|W(1 + |e|W/2m_0c^2)]^{-1/2} \qquad (2.5.2.12)$$
$$= \lambda_c(1 - \beta^2)^{1/2}/\beta, \qquad (2.5.2.13)$$

where λ_c is the Compton wavelength, $\lambda_c = h/m_0c = 0.0242$ Å, and

$$\sigma = 2\pi me\lambda/h^2 = (2\pi m_0 e/h^2)(\lambda_c/\beta)$$
$$= 2\pi/\{\lambda W[1 + (1 - \beta^2)^{1/2}]\}. \qquad (2.5.2.14)$$

Values for these quantities are listed in *IT* C (2004, Section 4.3.2). The variations of λ and σ with accelerating voltage are illustrated in Fig. 2.5.2.1. For high voltages, σ tends to a constant value, $2\pi m_0 e\lambda_c/h^2 = e/\hbar c$.

2.5.2.3. Recommended sign conventions

There are two alternative sets of signs for the functions describing wave optics. Both sets have been widely used in the literature. There is, however, a requirement for internal consistency within a particular analysis, independently of which set is adopted. Unfortunately, this requirement has not always been met and, in fact, it is only too easy at the outset of an analysis to make errors in this way. This problem might have come into prominence somewhat earlier were it not for the fact that, for centrosymmetric crystals (or indeed for centrosymmetric projections in the case of planar diffraction), only the signs used in the transmission and propagation functions can affect the results. It is not until the origin is set away from a centre of symmetry that there is a need to be consistent in every sign used.

Signs for electron diffraction have been chosen from two points of view: (1) defining as positive the sign of the exponent in the structure-factor expression and (2) defining the forward propagating free-space wavefunction with a positive exponent.

The second of these alternatives is the one which has been adopted in most solid-state and quantum-mechanical texts.

The first, or *standard crystallographic* convention, is the one which could most easily be adopted by crystallographers accustomed to retaining a positive exponent in the structure-factor equation. This also represents a consistent *International Tables* usage. It is, however, realized that both conventions will continue to be used in crystallographic computations, and that there are by now a large number of operational programs in use.

It is therefore recommended (*a*) that a particular sign usage be indicated as either *standard crystallographic* or *alternative crystallographic* to accord with Table 2.5.2.1, whenever there is a need for this to be explicit in publication, and (*b*) that either one or other of these systems be adhered to throughout an analysis in a self-consistent way, even in those cases where, as indicated above, some of the signs appear to have no effect on one particular conclusion.

2.5.2.4. Scattering of electrons by crystals; approximations

The forward-scattering approximation to the many-beam dynamical diffraction theory outlined in Chapter 5.2 provides the basis for the calculation of diffraction intensities and electron-microscope image contrast for thin crystals. [See Cowley (1995), Chapter 5.2 and *IT* C (2004) Sections 4.3.6 and 4.3.8.] On the other hand, there are various approximations which provide relatively simple analytical expressions, are useful for the determination of diffraction geometry, and allow estimates to be made of the relative intensities in diffraction patterns and electron micrographs in favourable cases.

(*a*) *The kinematical approximation*, derived in Section 2.5.2.2 from the first Born approximation, is analagous to the corresponding approximation of X-ray diffraction. It assumes that the scattering amplitudes are directly proportional to the three-dimensional Fourier transform of the potential distribution, $\varphi(\mathbf{r})$.

$$V(\mathbf{u}) = \int \varphi(\mathbf{r}) \exp\{2\pi i\mathbf{u} \cdot \mathbf{r}\}\, \mathrm{d}\mathbf{r}, \qquad (2.5.2.15)$$

so that the potential distribution $\varphi(\mathbf{r})$ takes the place of the charge-density distribution, $\rho(\mathbf{r})$, relevant for X-ray scattering.

The validity of the kinematical approximation as a basis for structure analysis is severely limited. For light-atom materials, such as organic compounds, it has been shown by Jap & Glaeser (1980) that the thickness for which the approximation gives reasonable accuracy for zone-axis patterns from single crystals is of the order of 100 Å for 100 keV electrons and increases, approximately as σ^{-1}, for higher energies. The thickness limits quoted for polycrystalline samples, having crystallite dimensions smaller than the sample thickness, are usually greater (Vainshtein, 1956). For heavy-atom materials the approximation is more limited since it may fail significantly for single heavy atoms.

(*b*) *The phase-object approximation* (POA), or high-voltage limit, is derived from the general many-beam dynamical

Table 2.5.2.1. *Standard crystallographic and alternative crystallographic sign conventions for electron diffraction*

	Standard	Alternative
Free-space wave	$\exp[-i(\mathbf{k}\cdot\mathbf{r}-\omega t)]$	$\exp[+i(\mathbf{k}\cdot\mathbf{r}-\omega t)]$
Fourier transforming from real space to reciprocal space	$\int \psi(\mathbf{r})\exp[+2\pi i(\mathbf{u}\cdot\mathbf{r})]\,\mathrm{d}\mathbf{r}$	$\int \psi(\mathbf{r})\exp[-2\pi i(\mathbf{u}\cdot\mathbf{r})]\,\mathrm{d}\mathbf{r}$
Fourier transforming from reciprocal space to real space	$\psi(\mathbf{r}) = \int \Psi(\mathbf{u})\exp[-2\pi i(\mathbf{u}\cdot\mathbf{r})]\,\mathrm{d}\mathbf{u}$	$\int \Psi(\mathbf{u})\exp[+2\pi i(\mathbf{u}\cdot\mathbf{r})]\,\mathrm{d}\mathbf{u}$
Structure factors	$V(\mathbf{h}) = (1/\Omega)\sum_j f_j(\mathbf{h})\exp(+2\pi i\mathbf{h}\cdot\mathbf{r}_j)$	$(1/\Omega)\sum_j f_j(\mathbf{h})\exp(-2\pi i\mathbf{h}\cdot\mathbf{r}_j)$
Transmission function (real space)	$\exp[-i\sigma\varphi(x,y)\Delta z]$	$\exp[+i\sigma\varphi(x,y)\Delta z]$
Phenomenological absorption	$\sigma\varphi(\mathbf{r}) - i\mu(\mathbf{r})$	$\sigma\varphi(\mathbf{r}) + i\mu(\mathbf{r})$
Propagation function $P(h)$ (reciprocal space) within the crystal	$\exp(-2\pi i\zeta_{\mathbf{h}}\Delta z)$	$\exp(+2\pi i\zeta_{\mathbf{h}}\Delta z)$
Iteration (reciprocal space)	$\Psi_{n+1}(\mathbf{h}) = [\Psi_n(\mathbf{h})\cdot P(\mathbf{h})] * Q(\mathbf{h})$	
Unitarity test (for no absorption)	$T(\mathbf{h}) = Q(\mathbf{h}) * Q^*(-\mathbf{h}) = \delta(\mathbf{h})$	
Propagation to the image plane-wave aberration function, where $\chi(U) = \pi\lambda\Delta f U^2 + \frac{1}{2}\pi C_s\lambda^3 U^4$, $U^2 = u^2 + v^2$ and Δf is positive for overfocus	$\exp[i\chi(U)]$	$\exp[-i\chi(U)]$

σ = electron interaction constant $= 2\pi me\lambda/h^2$; m = (relativistic) electron mass; λ = electron wavelength; e = (magnitude of) electron charge; h = Planck's constant; $k = 2\pi/\lambda$; Ω = volume of the unit cell; $\mathbf{u}$ = continuous reciprocal-space vector, components u, v; $\mathbf{h}$ = discrete reciprocal-space coordinate; $\varphi(x, y)$ = crystal potential averaged along beam direction (positive); Δz = slice thickness; $\mu(\mathbf{r})$ = absorption potential [positive; typically $\leq 0.1\sigma\varphi(\mathbf{r})$]; Δf = defocus (defined as negative for underfocus); C_s = spherical aberration coefficient; $\zeta_{\mathbf{h}}$ = excitation error relative to the incident-beam direction and defined as negative when the point h lies outside the Ewald sphere; $f_j(\mathbf{h})$ = atomic scattering factor for electrons, f_e, related to the atomic scattering factor for X-rays, f_X, by the Mott formula $f_e = (e/\pi U^2)(Z - f_X)$. $Q(\mathbf{h})$ = Fourier transform of periodic slice transmission function.

diffraction expression, equation (5.2.13.1), Chapter 5.2, by assuming the Ewald sphere curvature to approach zero. Then the scattering by a thin sample can be expressed by multiplying the incoming wave amplitude by the transmission function

$$q(xy) = \exp\{-i\sigma\varphi(xy)\}, \tag{2.5.2.16}$$

where $\varphi(xy) = \int \varphi(\mathbf{r})\,\mathrm{d}z$ is the projection of the potential distribution of the sample in the z direction, the direction of the incident beam. The diffraction-pattern amplitudes are then given by two-dimensional Fourier transform of (2.5.2.16).

This approximation is of particular value in relation to the electron microscopy of thin crystals. The thickness for its validity for 100 keV electrons is within the range 10 to 50 Å, depending on the accuracy and spatial resolution involved, and increases with accelerating voltage approximately as $\lambda^{-1/2}$. In computational work, it provides the starting point for the multislice method of dynamical diffraction calculations (*IT* C, 2004, Section 4.3.6.1).

(*c*) *The two-beam approximation* for dynamical diffraction of electrons assumes that only two beams, the incident beam and one diffracted beam (or two Bloch waves, each with two component amplitudes), exist in the crystal. This approximation has been adapted, notably by Hirsch *et al.* (1965), for use in the electron microscopy of inorganic materials.

It forms a convenient basis for the study of defects in crystals having small unit cells (metals, semiconductors *etc.*) and provides good preliminary estimates for the determination of crystal thicknesses and structure amplitudes for orientations well removed from principal axes, and for electron energies up to 200–500 keV, but it has decreasing validity, even for favourable cases, for higher energies. It has been used in the past as an 'extinction correction' for powder-pattern intensities (Vainshtein, 1956).

(*d*) *The Bethe second approximation*, proposed by Bethe (1928) as a means for correcting the two-beam approximation for the effects of weakly excited beams, replaces the Fourier coefficients of potential by the 'Bethe potentials'

$$U_{\mathbf{h}} = V_{\mathbf{h}} - 2k_0\sigma\sum_{\mathbf{g}}\frac{V_{\mathbf{g}}\cdot V_{\mathbf{h}-\mathbf{g}}}{\kappa^2 - k_{\mathbf{g}}^2}. \tag{2.5.2.17}$$

Use of these potentials has been shown to account well for the deviations of powder-pattern intensities from the predictions of two-beam theory (Horstmann & Meyer, 1965) and to predict accurately the extinctions of Kikuchi lines at particular accelerating voltages due to relativistic effects (Watanabe *et al.*, 1968), but they give incorrect results for the small-thickness limit.

2.5.2.5. Kinematical diffraction formulae

(1) *Comparison with X-ray diffraction.* The relations of real-space and reciprocal-space functions are analogous to those for X-ray diffraction [see equations (2.5.2.2), (2.5.2.10) and (2.5.2.15)]. For diffraction by crystals

$$\varphi(\mathbf{r}) = \sum_{\mathbf{h}} V_{\mathbf{h}}\exp\{-2\pi i\mathbf{h}\cdot\mathbf{r}\},$$

$$V_{\mathbf{h}} = \int \varphi(\mathbf{r})\exp\{2\varphi i\mathbf{h}\cdot\mathbf{r}\}\,\mathrm{d}\mathbf{r} \tag{2.5.2.18}$$

$$= \frac{1}{\Omega}\sum_i f_i(\mathbf{h})\exp\{2\pi i\mathbf{h}\cdot\mathbf{r}_i\}, \tag{2.5.2.19}$$

where the integral of (2.5.2.18) and the summation of (2.5.2.19) are taken over one unit cell of volume (see Dawson *et al.*, 1974).

Important differences from the X-ray case arise because

(*a*) the wavelength is relatively small so that the Ewald-sphere curvature is small in the reciprocal-space region of appreciable scattering amplitude;

(*b*) the dimensions of the single-crystal regions giving appreciable scattering amplitudes are small so that the 'shape transform' regions of scattering power around the reciprocal-lattice points are relatively large;

(*c*) the spread of wavelengths is small (10^{-5} or less, with no white-radiation background) and the degree of collimation is better (10^{-4} to 10^{-6}) than for conventional X-ray sources.

As a consequence of these factors, single-crystal diffraction patterns may show many simultaneous reflections, representing almost-planar sections of reciprocal space, and may show fine structure or intensity variations reflecting the crystal dimensions and shape.

(2) Kinematical diffraction-pattern intensities are calculated in a manner analogous to that for X-rays except that

(*a*) no polarization factor is included because of the small-angle scattering conditions;

(*b*) integration over regions of scattering power around reciprocal-lattice points cannot be assumed unless appropriate experimental conditions are ensured.

For a thin, flat, lamellar crystal of thickness H, the observed intensity is

$$I_{\mathbf{h}}/I_{\mathbf{0}} = |\sigma(V_{\mathbf{h}}/\Omega)(\sin \pi\zeta_{\mathbf{h}} H)/(\pi\zeta_{\mathbf{h}})|^2, \tag{2.5.2.20}$$

where $\zeta_{\mathbf{h}}$ is the excitation error for the $\mathbf{h}$ reflection and Ω is the unit-cell volume.

For a single-crystal diffraction pattern obtained by rotating a crystal or from a uniformly bent crystal or for a mosaic crystal with a uniform distribution of orientations, the intensity is

$$I_{\mathbf{h}} = I_{\mathbf{0}} \frac{\sigma^2 |V_{\mathbf{h}}|^2 V_{\mathrm{c}} d_{\mathbf{h}}}{4\pi^2 \Omega^2}, \tag{2.5.2.21}$$

where V_{c} is the crystal volume and $d_{\mathbf{h}}$ is the lattice-plane spacing. For a polycrystalline sample of randomly oriented small crystals, the intensity per unit length of the diffraction ring is

$$I_{\mathbf{h}} = I_{\mathbf{0}} \frac{\sigma^2 |V_{\mathbf{h}}|^2 V_{\mathrm{c}} d_{\mathbf{h}}^2 M_{\mathbf{h}}}{8\pi^2 \Omega^2 L\lambda}, \tag{2.5.2.22}$$

where $M_{\mathbf{h}}$ is the multiplicity factor for the $\mathbf{h}$ reflection and L is the camera length, or the distance from the specimen to the detector plane. The special cases of 'oblique texture' patterns from powder patterns having preferred orientations are treated in *IT* C (2004, Section 4.3.5).

(3) *Two-beam dynamical diffraction formulae: complex potentials including absorption.* In the two-beam dynamical diffraction approximation, the intensities of the directly transmitted and diffracted beams for transmission through a crystal of thickness H, in the absence of absorption, are

$$I_{\mathbf{0}} = (1 + w^2)^{-1} \left[w^2 + \cos^2 \left\{ \frac{\pi H (1 + w^2)^{1/2}}{\xi_{\mathbf{h}}} \right\} \right] \tag{2.5.2.23}$$

$$I_{\mathbf{h}} = (1 + w^2)^{-1} \sin^2 \left\{ \frac{\pi H (1 + w^2)^{1/2}}{\xi_{\mathbf{h}}} \right\}, \tag{2.5.2.24}$$

where $\xi_{\mathbf{h}}$ is the extinction distance, $\xi_{\mathbf{h}} = (2\sigma|V_{\mathbf{h}}|)^{-1}$, and

$$w = \xi_{\mathbf{h}} \zeta_{\mathbf{h}} = \Delta\theta/(2\sigma|V_{\mathbf{h}}|d_{\mathbf{h}}), \tag{2.5.2.25}$$

where $\Delta\theta$ is the deviation from the Bragg angle.

For the case that $\zeta_{\mathbf{h}} = 0$, with the incident beam at the Bragg angle, this reduces to the simple *Pendellösung* expression

$$I_{\mathbf{h}} = 1 - I_{\mathbf{0}} = \sin^2\{2\pi\sigma|V_{\mathbf{h}}|H\}. \tag{2.5.2.26}$$

The effects on the elastic Bragg scattering amplitudes of the inelastic or diffuse scattering may be introduced by adding an out-of-phase component to the structure amplitudes, so that for a centrosymmetric crystal, $V_{\mathbf{h}}$ becomes complex by addition of an imaginary component. Alternatively, an absorption function $\mu(\mathbf{r})$, having Fourier coefficients $\mu_{\mathbf{h}}$, may be postulated so that $\sigma V_{\mathbf{h}}$ is replaced by $\sigma V_{\mathbf{h}} + i\mu_{\mathbf{h}}$. The $\mu_{\mathbf{h}}$ are known as phenomenological absorption coefficients and their validity in many-beam diffraction has been demonstrated by, for example, Rez (1978).

The magnitudes $\mu_{\mathbf{h}}$ depend on the nature of the experiment and the extent to which the various inelastically or diffusely scattered electrons are included in the measurements being made. If measurements are made of purely elastic scattering intensities for Bragg reflections or of image intensity variations due to the interaction of the sharp Bragg reflections only, the main contributions to the absorption coefficients are as follows (Radi, 1970):

(*a*) from plasmon and single-electron excitations, $\mu_{\mathbf{0}}$ is of the order of 0.1 $V_{\mathbf{0}}$ and $\mu_{\mathbf{h}}$, for $\mathbf{h} \neq 0$, is negligibly small;

(*b*) from thermal diffuse scattering; $\mu_{\mathbf{h}}$ is of the order of 0.1 $V_{\mathbf{h}}$ and decreasing more slowly than $V_{\mathbf{h}}$ with scattering angle.

Including absorption effects in (2.5.2.26) for the case $\zeta_{\mathbf{h}} = 0$ gives

$$\begin{aligned} I_{\mathbf{0}} &= \tfrac{1}{2}\exp\{-\mu_{\mathbf{0}} H\}[\cosh \mu_{\mathbf{h}} H + \cos(2\pi\sigma V_{\mathbf{h}} H)], \\ I_{\mathbf{h}} &= \tfrac{1}{2}\exp\{-\mu_{\mathbf{0}} H\}[\cosh \mu_{\mathbf{h}} H - \cos(2\pi\sigma V_{\mathbf{h}} H)]. \end{aligned} \tag{2.5.2.27}$$

The Borrmann effect is not very pronounced for electrons because $\mu_{\mathbf{h}} \ll \mu_{\mathbf{0}}$, but can be important for the imaging of defects in thick crystals (Hirsch *et al.*, 1965; Hashimoto *et al.*, 1961).

Attempts to obtain analytical solutions for the dynamical diffraction equations for more than two beams have met with few successes. There are some situations of high symmetry, with incident beams in exact zone-axis orientations, for which the many-beam solution can closely approach equivalent two- or three-beam behaviour (Fukuhara, 1966). Explicit solutions for the three-beam case, which displays some aspects of many-beam character, have been obtained (Gjønnes & Høier, 1971; Hurley & Moodie, 1980).

2.5.2.6. Imaging with electrons

Electron optics. Electrons may be focused by use of axially symmetric magnetic fields produced by electromagnetic lenses. The focal length of such a lens used as a projector lens (focal points outside the lens field) is given by

$$f_{\mathrm{p}}^{-1} = \frac{e}{8mW_{\mathrm{r}}} \int_{-\infty}^{\infty} H_z^2(z)\,\mathrm{d}z, \tag{2.5.2.28}$$

where W_{r} is the relativistically corrected accelerating voltage and H_z is the z component of the magnetic field. An expression in terms of experimental constants was given by Liebman (1955) as

$$\frac{1}{f} = \frac{A_0 (NI)^2}{W_{\mathrm{r}}(S + D)}, \tag{2.5.2.29}$$

where A_0 is a constant, NI is the number of ampere turns of the lens winding, S is the length of the gap between the magnet pole pieces and D is the bore of the pole pieces.

Lenses of this type have irreducible aberrations, the most important of which for the paraxial conditions of electron microscopy is the third-order spherical aberration, coefficient C_{s}, giving a variation of focal length of $C_{\mathrm{s}}\alpha^2$ for a beam at an angle α to the axis. Chromatic aberration, coefficient C_{c}, gives a spread of focal lengths

$$\Delta f = C_{\mathrm{c}} \left(\frac{\Delta W_0}{W_0} + 2\frac{\Delta I}{I} \right) \tag{2.5.2.30}$$

for variations ΔW_0 and ΔI of the accelerating voltage and lens currents, respectively.

The objective lens of an electron microscope is the critical lens for the determination of image resolution and contrast. The action of this lens in a conventional transmission electron microscope (TEM) is described by use of the Abbe theory for coherent incident illumination transmitted through the object to produce a wavefunction $\psi_0(xy)$ (see Fig. 2.5.2.2).

The amplitude distribution in the back focal plane of the objective lens is written

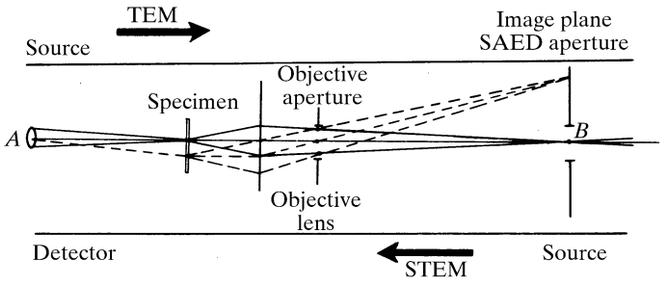

Fig. 2.5.2.2. Diagram representing the critical components of a conventional transmission electron microscope (TEM) and a scanning transmission electron microscope (STEM). For the TEM, electrons from a source A illuminate the specimen and the objective lens forms an image of the transmitted electrons on the image plane, B. For the STEM, a source at B is imaged by the objective lens to form a small probe on the specimen and some part of the transmitted beam is collected by a detector at A.

$$\Psi_0(u, v) \cdot T(u, v), \tag{2.5.2.31}$$

where $\Psi_0(u, v)$ is the Fourier transform of $\psi_0(x, y)$ and $T(u, v)$ is the transfer function of the lens, consisting of an aperture function

$$A(u, v) = \begin{cases} 1 & \text{for } (u^2 + v^2)^{1/2} \leq A \\ 0 & \text{elsewhere} \end{cases} \tag{2.5.2.32}$$

and a phase function $\exp\{i\chi(u, v)\}$ where the phase perturbation $\chi(uv)$ due to lens defocus Δf and aberrations is usually approximated as

$$\chi(uv) = \pi \cdot \Delta f \cdot \lambda(u^2 + v^2) + \frac{\pi}{2} C_s \lambda^3 (u^2 + v^2)^2, \tag{2.5.2.33}$$

and u, v are the reciprocal-space variables related to the scattering angles φ_x, φ_y by

$$u = (\sin \varphi_x)/\lambda,$$
$$v = (\sin \varphi_y)/\lambda.$$

The image amplitude distribution, referred to the object coordinates, is given by Fourier transform of (2.5.2.31) as

$$\psi(xy) = \psi_0(xy) * t(xy), \tag{2.5.2.34}$$

where $t(xy)$, given by Fourier transform of $T(u, v)$, is the spread function. The image intensity is then

$$I(xy) = |\psi(xy)|^2 = |\psi_0(xy) * t(xy)|^2. \tag{2.5.2.35}$$

In practice the coherent imaging theory provides a good approximation but limitations of the coherence of the illumination have appreciable effects under high-resolution imaging conditions.

The variation of focal lengths according to (2.5.2.30) is described by a function $G(\Delta f)$. Illumination from a finite incoherent source gives a distribution of incident-beam angles $H(u_1, v_1)$. Then the image intensity is found by integrating incoherently over Δf and u_1, v_1:

$$I(xy) = \int\int G(\Delta f) \cdot H(u_1 v_1) \times |\mathscr{F}\{\Psi_0(u - u_1, v - v_1) \cdot T_{\Delta f}(u, v)\}|^2 \, \mathrm{d}(\Delta f) \cdot \mathrm{d}u_1 \, \mathrm{d}v_1, \tag{2.5.2.36}$$

where $\mathscr{F}$ denotes the Fourier-transform operation.

In the scanning transmission electron microscope (STEM), the objective lens focuses a small bright source of electrons on the object and directly transmitted or scattered electrons are detected to form an image as the incident beam is scanned over the object (see Fig. 2.5.2.2). Ideally the image amplitude can be related to that of the conventional transmission electron microscope by use of the 'reciprocity relationship' which refers to point sources and detectors for scalar radiation in scalar fields with elastic scattering processes only. It may be stated: 'The amplitude at a point B due to a point source at A is identical to that which would be produced at A for the identical source placed at B'.

For an axial point source, the amplitude distribution produced by the objective lens on the specimen is

$$\mathscr{F}[T(u, v)] = t(xy). \tag{2.5.2.37}$$

If this is translated by the scan to X, Y, the transmitted wave is

$$\psi_0(xy) = q(xy) \cdot t(x - X, y - Y). \tag{2.5.2.38}$$

The amplitude on the plane of observation following the specimen is then

$$\Psi(uv) = Q(u, v) * \{T(uv) \exp[2\pi i(uX + vY)]\}, \tag{2.5.2.39}$$

and the image signal produced by a detector having a sensitivity function $H(u, v)$ is

$$I(X, Y) = \int H(u, v) |Q(u, v) * T(u, v) \times \exp\{2\pi i(uX + vY)\}|^2 \, \mathrm{d}u \, \mathrm{d}v. \tag{2.5.2.40}$$

If $H(u, v)$ represents a small detector, approximated by a delta function, this becomes

$$I(x, y) = |q(xy) * t(xy)|^2, \tag{2.5.2.41}$$

which is identical to the result (2.5.2.35) for a plane incident wave in the conventional transmission electron microscope.

2.5.2.7. Imaging of very thin and weakly scattering objects

(*a*) *The weak-phase-object approximation.* For sufficiently thin objects, the effect of the object on the incident-beam amplitude may be represented by the transmission function (2.5.2.16) given by the phase-object approximation. If the fluctuations, $\varphi(xy) - \bar{\varphi}$, about the mean value of the projected potential are sufficiently small so that $\sigma[\varphi(xy) - \bar{\varphi}] \ll 1$, it is possible to use the *weak-phase-object approximation* (WPOA)

$$q(xy) = \exp\{-i\sigma\varphi(xy)\} = 1 - i\sigma\varphi(xy), \tag{2.5.2.42}$$

where $\varphi(xy)$ is referred to the average value, $\bar{\varphi}$. The assumption that only first-order terms in $\sigma\varphi(xy)$ need be considered is the equivalent of a single-scattering, or kinematical, approximation applied to the two-dimensional function, the projected potential

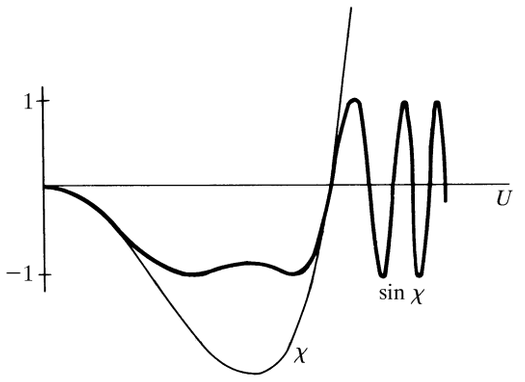

Fig. 2.5.2.3. The functions $\chi(U)$, the phase factor for the transfer function of a lens given by equation (2.5.2.33), and $\sin\chi(U)$ for the Scherzer optimum defocus condition, relevant for weak phase objects, for which the minimum value of $\chi(U)$ is $-2\pi/3$.

of (2.5.2.16). From (2.5.2.42), the image intensity (2.5.2.35) becomes

$$I(xy) = 1 + 2\sigma\varphi(xy) * s(xy), \tag{2.5.2.43}$$

where the spread function $s(xy)$ is the Fourier transform of the imaginary part of $T(uv)$, namely $A(uv)\sin\chi(uv)$.

The optimum imaging condition is then found, following Scherzer (1949), by specifying that the defocus should be such that $|\sin\chi|$ is close to unity for as large a range of $U = (u^2 + v^2)^{1/2}$ as possible. This is so for a negative defocus such that $\chi(uv)$ decreases to a minimum of about $-2\pi/3$ before increasing to zero and higher as a result of the fourth-order term of (2.5.2.33) (see Fig. 2.5.2.3). This optimum, 'Scherzer defocus' value is given by

$$\frac{\mathrm{d}\chi}{\mathrm{d}u} = 0 \quad \text{for} \quad \chi = -2\pi/3$$

or

$$\Delta f = -\left(\tfrac{4}{3} C_\mathrm{s}\lambda\right)^{1/2}. \tag{2.5.2.44}$$

The resolution limit is then taken as corresponding to the value of $U = 1.51 C_\mathrm{s}^{-1/4}\lambda^{-3/4}$ when $\sin\chi$ becomes zero, before it begins to oscillate rapidly with U. The resolution limit is then

$$\Delta x = 0.66 C_\mathrm{s}^{1/4}\lambda^{3/4}. \tag{2.5.2.45}$$

For example, for $C_\mathrm{s} = 1$ mm and $\lambda = 2.51 \times 10^{-2}$ Å (200 keV), $\Delta x = 2.34$ Å.

Within the limits of the WPOA, the image intensity can be written simply for a number of other imaging modes in terms of the Fourier transforms $c(\mathbf{r})$ and $s(\mathbf{r})$ of the real and imaginary parts of the objective-lens transfer function $T(\mathbf{u}) = A(\mathbf{u})\exp\{i\chi(\mathbf{u})\}$, where $\mathbf{r}$ and $\mathbf{u}$ are two-dimensional vectors in real and reciprocal space, respectively.

For dark-field TEM images, obtained by introducing a central stop to block out the central beam in the diffraction pattern in the back-focal plane of the objective lens,

$$I(\mathbf{r}) = [\sigma\varphi(\mathbf{r}) * c(\mathbf{r})]^2 + [\sigma\varphi(\mathbf{r}) * s(\mathbf{r})]^2. \tag{2.5.2.46}$$

Here, as in (2.5.2.42), $\varphi(\mathbf{r})$ should be taken to imply the difference from the mean potential value, $\varphi(\mathbf{r}) - \bar{\varphi}$.

For bright-field STEM imaging with a very small detector placed axially in the central beam of the diffraction pattern (2.5.2.39) on the detector plane, the intensity, from (2.5.2.41), is given by (2.5.2.43).

For a finite axially symmetric detector, described by $D(\mathbf{u})$, the image intensity is

$$I(\mathbf{r}) = 1 + 2\sigma\varphi(\mathbf{r}) * \{s(\mathbf{r})[d(\mathbf{r}) * c(\mathbf{r})] - c(\mathbf{r})[d(\mathbf{r}) * s(\mathbf{r})]\}, \tag{2.5.2.47}$$

where $d(\mathbf{r})$ is the Fourier transform of $D(\mathbf{u})$ (Cowley & Au, 1978).

For STEM with an annular dark-field detector which collects all electrons scattered outside the central spot of the diffraction pattern in the detector plane, it can be shown that, to a good approximation (valid except near the resolution limit)

$$I(\mathbf{r}) = \sigma^2\varphi^2(\mathbf{r}) * [c^2(\mathbf{r}) + s^2(\mathbf{r})]. \tag{2.5.2.48}$$

Since $c^2(\mathbf{r}) + s^2(\mathbf{r}) = |t(\mathbf{r})|^2$ is the intensity distribution of the electron probe incident on the specimen, (2.5.2.48) is equivalent to the incoherent imaging of the function $\sigma^2\varphi^2(\mathbf{r})$.

Within the range of validity of the WPOA or, in general, whenever the zero beam of the diffraction pattern is very much stronger than any diffracted beam, the general expression (2.5.2.36) for the modifications of image intensities due to limited coherence may be conveniently approximated. The effect of integrating over the variables $\Delta f, u_1, v_1$, may be represented by multiplying the transfer function $T(u, v)$ by so-called 'envelope functions' which involve the Fourier transforms of the functions $G(\Delta f)$ and $H(u_1, v_1)$.

For example, if $G(\Delta f)$ is approximated by a Gaussian of width ε (at e^{-1} of the maximum) centred at Δf_0 and $H(u_1 v_1)$ is a circular aperture function

$$H(u_1 v_1) = \begin{cases} 1 & \text{if } u_1, v_1 < b \\ 0 & \text{otherwise,} \end{cases}$$

the transfer function $T_0(uv)$ for coherent radiation is multiplied by

$$\exp\{-\pi^2\lambda^2\varepsilon^2(u^2 + v^2)^2/4\} \cdot J_1(\pi B\eta)/(\pi B\eta)$$

where

$$\eta = f_0\lambda(u + v) + C_\mathrm{s}\lambda^3(u^3 + v^3) + \pi i\varepsilon^2\lambda^2(u^3 + u^2 v + uv^2 + v^3)/2. \tag{2.5.2.49}$$

(*b*) *The projected charge-density approximation.* For very thin specimens composed of moderately heavy atoms, the WPOA is inadequate. Within the region of validity of the phase-object approximation (POA), more complicated relations analagous to (2.5.2.43) to (2.5.2.47) may be written. A simpler expression may be obtained by use of the two-dimensional form of Poisson's equation, relating the projected potential distribution $\varphi(xy)$ to the projected charge-density distribution $\rho(xy)$. This is the PCDA (projected charge-density approximation) (Cowley & Moodie, 1960),

$$I(xy) = 1 + 2\Delta f \cdot \lambda\sigma\rho(xy). \tag{2.5.2.50}$$

This is valid for sufficiently small values of the defocus Δf, provided that the effects of the spherical aberration may be neglected, *i.e.* for image resolutions not too close to the Scherzer

resolution limit (Lynch *et al.*, 1975). The function $\rho(xy)$ includes contributions from both the positive atomic nuclei and the negative electron clouds. For underfocus (Δf negative), single atoms give dark spots in the image. The contrast reverses with defocus.

2.5.2.8. Crystal structure imaging

(*a*) *Introduction.* It follows from (2.5.2.43) and (2.5.2.42) that, within the severe limitations of validity of the WPOA or the PCDA, images of very thin crystals, viewed with the incident beam parallel to a principal axis, will show dark spots at the positions of rows of atoms parallel to the incident beam. Provided that the resolution limit is less than the projected distances between atom rows (1–3 Å), the projection of the crystal structure may be seen directly.

In practice, theoretical and experimental results suggest that images may give a direct, although nonlinear, representation of the projected potential or charge-density distribution for thicknesses much greater than the thicknesses for validity of these approximations, *e.g.* for thicknesses which may be 50 to 100 Å for 100 keV electrons for 3 Å resolutions and which increase for comparable resolutions at higher voltage but decrease with improved resolutions.

The use of high-resolution imaging as a means for determining the structures of crystals and for investigating the form of the defects in crystals in terms of the arrangement of the atoms has become a widely used and important branch of crystallography with applications in many areas of solid-state science. It must be emphasized, however, that image intensities are strongly dependent on the crystal thickness and orientation and also on the instrumental parameters (defocus, aberrations, alignment *etc.*). It is only when all of these parameters are correctly adjusted to lie within strictly defined limits that interpretation of images in terms of atom positions can be attempted [see *IT* C (2004, Section 4.3.8)].

Reliable interpretations of high-resolution images of crystals ('crystal structure images') may be made, under even the most favourable circumstances, only by the comparison of observed image intensities with intensities calculated by use of an adequate approximation to many-beam dynamical diffraction theory [see *IT* C (2004, Section 4.3.6)]. Most calculations for moderate or large unit cells are currently made by the multislice method based on formulation of the dynamical diffraction theory due to Cowley & Moodie (1957). For smaller unit cells, the matrix method based on the Bethe (1928) formulation is also frequently used (Hirsch *et al.*, 1965).

(*b*) *Fourier images.* For periodic objects in general, and crystals in particular, the amplitudes of the diffracted waves in the back focal plane are given from (2.5.2.31) by

$$\Psi_0(\mathbf{h}) \cdot T(\mathbf{h}). \qquad (2.5.2.51)$$

For rectangular unit cells of the projected unit cell, the vector $\mathbf{h}$ has components h/a and k/b. Then the set of amplitudes (2.5.2.34), and hence the image intensities, will be identical for two different sets of defocus and spherical aberration values Δf_1, C_{s1} and Δf_2, C_{s2} if, for an integer N,

$$\chi_1(h) = \chi_2(h) = 2N\pi;$$

i.e.

$$\pi\lambda\left(\frac{h^2}{a^2}+\frac{k^2}{b^2}\right)(\Delta f_1 - \Delta f_2) + \frac{1}{2}\pi\lambda^3\left(\frac{h^2}{a^2}+\frac{k^2}{b^2}\right)^2 (C_{s1} - C_{s2}) = 2\pi N.$$

This relationship is satisfied for all h, k if a^2/b^2 is an integer and

$$\Delta f_1 - \Delta f_2 = 2na^2/\lambda$$

and

$$C_{s1} - C_{s2} = 4ma^4/\lambda^3, \qquad (2.5.2.52)$$

where m, n are integers (Kuwabara, 1978). The relationship for Δf is an expression of the Fourier image phenomenon, namely that for a plane-wave incidence, the intensity distribution for the image of a periodic object repeats periodically with defocus (Cowley & Moodie, 1960). Hence it is often necessary to define the defocus value by observation of a nonperiodic component of the specimen such as a crystal edge (Spence *et al.*, 1977).

For the special case $a^2 = b^2$, the image intensity is also reproduced exactly for

$$\Delta f_1 - \Delta f_2 = (2n+1)a^2/\lambda, \qquad (2.5.2.53)$$

except that in this case the image is translated by a distance $a/2$ parallel to each of the axes.

2.5.2.9. Image resolution

(1) *Definition and measurement.* The 'resolution' of an electron microscope or, more correctly, the 'least resolvable distance', is usually defined by reference to the transfer function for the coherent imaging of a weak phase object under the Scherzer optimum defocus condition (2.5.2.44). The resolution figure is taken as the inverse of the U value for which $\sin\chi(U)$ first crosses the axis and is given, as in (2.5.2.45), by

$$\Delta x = 0.66C_s^{1/4}\lambda^{3/4}. \qquad (2.5.2.45)$$

It is assumed that an objective aperture is used to eliminate the contribution to the image for U values greater than the first zero crossing, since for these contributions the relative phases are distorted by the rapid oscillations of $\sin\chi(U)$ and the corresponding detail of the image is not directly interpretable in terms of the projection of the potential distribution of the object.

The resolution of the microscope in practice may be limited by the incoherent factors which have the effect of multiplying the WPOA transfer function by envelope functions as in (2.5.2.49).

The resolution, as defined above, and the effects of the envelope functions may be determined by Fourier transform of the image of a suitable thin, weakly scattering amorphous specimen. The Fourier-transform operation may be carried out by use of an optical diffractometer. A more satisfactory practice is to digitize the image directly by use of a two-dimensional detector system in the microscope or from a photographic recording, and perform the Fourier transform numerically.

For the optical diffractometer method, the intensity distribution obtained is given from (2.5.2.43) as a radially symmetric function of U,

$$\begin{aligned} I(U) &= |\mathscr{F} I(xy)|^2 \\ &= \delta(U) + 4\sigma^2|\Phi(u)|^2 \cdot \sin^2\chi(U) \cdot E^2(U), \end{aligned} \qquad (2.5.2.54)$$

where $E(U)$ is the product of the envelope functions.

In deriving (2.5.2.54) it has been assumed that:

(*a*) the WPOA applies;

(*b*) the optical transmission function of the photographic record is linearly related to the image intensity, $I(xy)$;

(*c*) the diffraction intensity $|\Phi(U)|^2$ is a radially symmetric, smoothly varying function such as is normally produced by a sufficiently large area of the image of an amorphous material;

(*d*) there is no astigmatism present and no drift of the specimen; either of these factors would remove the radial symmetry.

From the form of (2.5.2.54) and a preknowledge of $|\Phi(U)|^2$, the zero crossings of $\sin\chi$ and the form of $E(U)$ may be deduced. Analysis of a through-focus series of images provides more complete and reliable information.

(2) Detail on a scale much smaller than the resolution of the electron microscope, as defined above, is commonly seen in electron micrographs, especially for crystalline samples. For example, lattice fringes, having the periodicity of the crystal lattice planes, with spacings as small as 0.6 Å in one direction, have been observed using a microscope having a resolution of about 2.5 Å (Matsuda *et al.*, 1978), and two-dimensionally periodic images showing detail on the scale of 0.5 to 1 Å have been observed with a similar microscope (Hashimoto *et al.*, 1977).

Such observations are possible because

(*a*) for periodic objects the diffraction amplitude $\Psi_0(uv)$ in (2.5.2.31) is a set of delta functions which may be multiplied by the corresponding values of the transfer function that will allow strong interference effects between the diffracted beams and the zero beam, or between different diffracted beams;

(*b*) the envelope functions for the WPOA, arising from incoherent imaging effects, do not apply for strongly scattering crystals; the more general expression (2.5.2.36) provides that the incoherent imaging factors will have much less effect on the interference of some sets of diffracted beams.

The observation of finely spaced lattice fringes provides a measure of some important factors affecting the microscope performance, such as the presence of mechanical vibrations, electrical interference or thermal drift of the specimen. A measure of the fineness of the detail observable in this type of image may therefore be taken as a measure of 'instrumental resolution'.

2.5.2.10. Electron diffraction in electron microscopes

Currently most electron-diffraction patterns are obtained in conjunction with images, in electron microscopes of one form or another, as follows.

(*a*) Selected-area electron-diffraction (SAED) patterns are obtained by using intermediate and projector lenses to form an image of the diffraction pattern in the back-focal plane of the objective lens (Fig. 2.5.2.2). The area of the specimen from which the diffraction pattern is obtained is defined by inserting an aperture in the image plane of the objective lens. For parallel illumination of the specimen, sharp diffraction spots are produced by perfect crystals.

A limitation to the area of the specimen from which the diffraction pattern can be obtained is imposed by the spherical aberration of the objective lens. For a diffracted beam scattered through an angle α, the spread of positions in the object for which the diffracted beam passes through a small axial aperture in the image plane is $C_s\alpha^3$, *e.g.* for $C_s = 1$ mm, $\alpha = 5 \times 10^{-2}$ rad (10,0,0 reflection from gold for 100 keV electrons), $C_s\alpha^3 = 1250$ Å, so that a selected-area diameter of less than about 2000 Å is not feasible. For higher voltages, the minimum selected-area diameter decreases with λ^2 if the usual assumption is made that C_s increases for higher-voltage microscopes so that $C_s\lambda$ is a constant.

(*b*) Convergent-beam electron-diffraction (CBED) patterns are obtained when an incident convergent beam is focused on the specimen, as in an STEM instrument or an STEM attachment for a conventional TEM instrument.

For a large, effectively incoherent source, such as a conventional hot-filament electron gun, the intensities are added for each incident-beam direction. The resulting CBED pattern has an intensity distribution

$$I(uv) = \int |\Psi_{u_1v_1}(uv)|^2 \, \mathrm{d}u_1 \, \mathrm{d}v_1, \qquad (2.5.2.55)$$

where $\Psi_{u_1v_1}(uv)$ is the Fourier transform of the exit wave at the specimen for an incident-beam direction u_1, v_1.

(*c*) Coherent illumination from a small bright source such as a field emission gun may be focused on the specimen to give an electron probe having an intensity distribution $|t(xy)|^2$ and a diameter equal to the STEM dark-field image resolution [equation (2.5.2.47)] of a few Å. The intensity distribution of the resulting microdiffraction pattern is then

$$|\Psi(uv)|^2 = |\Psi_0(uv) * T(uv)|^2, \qquad (2.5.2.56)$$

where $\Psi_0(uv)$ is the Fourier transform of the exit wave at the specimen. Interference occurs between waves scattered from the various incident-beam directions. The diffraction pattern is thus an in-line hologram as envisaged by Gabor (1949).

(*d*) Diffraction patterns may be obtained by using an optical diffractometer (or computer) to produce the Fourier transform squared of a small selected region of a recorded image. The optical diffraction-pattern intensity obtained under the ideal conditions specified under equation (2.5.2.54) is given, in the case of weak phase objects, by

$$I(uv) = \delta(uv) + 4\sigma^2|\Phi(uv)|^2 \cdot \sin^2\chi(uv) \cdot E^2(uv) \qquad (2.5.2.57)$$

or, more generally, by

$$I(uv) = c\delta(uv) + |\Psi(uv) \cdot T(uv) * \Psi^*(uv) \cdot T^*(uv)|^2,$$

where $\Psi(uv)$ is the Fourier transform of the wavefunction at the exit face of the specimen and c is a constant depending on the characteristics of the photographic recording medium.

2.5.3. Point-group and space-group determination by convergent-beam electron diffraction

By M. Tanaka

2.5.3.1. Introduction

Because the cross section for electron scattering is at least a thousand times greater than that for X-rays, and because multiple Bragg scattering preserves information on symmetry (such as the absence of inversion symmetry), electron diffraction is exquisitely sensitive to symmetry. The additional ability of modern electron-optical lenses to focus an electron probe down to nanometre dimensions, and so allow the study of nanocrystals too small for analysis by X-rays, has meant that the method of convergent-beam diffraction described here has now become the preferred method of symmetry determination for very small crystals, domains, twinned structures, quasicrystals, incommensurate structures and other imperfectly crystalline materials.

Convergent-beam electron diffraction (CBED) originated with the experiments of Kossel & Möllenstedt (1938). However, modern crystallographic investigations by CBED began with the studies performed by Goodman & Lehmpfuhl (1965) in a modified transmission electron microscope. They obtained CBED patterns by converging a conical electron beam with an angle of more than 10^{-3} rad on an ~30 nm diameter specimen area, which had uniform thickness and no bending. Instead of the